Growth of Dihydrotetraazapentacene Layers on Cu(110)

Anthony Thomas, Walter Malone, Thomas Leoni, Alain Ranguis, Zhongrui Chen, Olivier Siri, Abdelkader Kara, Peter Zeppenfeld, Conrad Becker

Growth of Dihydrotetraazapentacene Layers on Cu(110)

Anthony Thomas[a], Walter Malone[b], Thomas Leoni[a], Alain Ranguis[a], Zhongrui Chen[a], Olivier Siri[a], Abdelkader Kara[b], Peter Zeppenfeld[a,c] and Conrad Becker[a,*].

[a]Aix-Marseille University, CNRS, CINaM, UMR 7325, 13288 Marseille, France.
[b]Department of Physics, University of Central Florida, Orlando, Florida 32816, United States.
[c]Institute of Experimental Physics, Johannes Kepler University Linz, Altenberger Str. 69, A-4040 Linz, Austria.

*corresponding author: conrad.becker@univ-amu.fr

ABSTRACT: The adsorption of 5,14-dihydro-5,7,12,14-tetraazapentacene (DHTAP) on Cu(110) has been investigated at different temperatures and coverages by means of scanning tunneling microscopy (STM) and low-energy diffraction (LEED). Our results show that the interaction of DHTAP with the Cu(110) surface differs considerably from that of pentacene on the same surface. The DHTAP molecules are chemisorbed on the surface via strong Cu-N bonds with an adsorption energy of roughly 3eV per molecule twice as high as the value for pentacene. We could identify three different ordered superstructures, which are commensurate with the substrate and characterized by the matrices (6 -1 | 1 2), (7 0 | 1 2) and (6 0 | 1 2), respectively.

Introduction:

Organic semiconductors can today be found in a wide range of applications in microelectronics and most notably as organic light emitting diodes (OLED)[1–3] in the displays of smartphones and TV screens. In this context pentacene (**1** in Scheme 1) films have often been used as a benchmark material because of a charge carrier mobility, which is comparable to that of amorphous silicon[4]. Already in 2007 Koch pointed out that the hybrid organic-metal interface is a determining factor for the performance of devices because of its influence on the growth of extended multilayers or thin films and the electronic properties of the interface, which influence charge carrier injection[5]. We here address this question for a derivative of pentacene: 5,14-dihydro-5,7,12,14-tetraazapentacene (DHTAP, **2** in scheme 1). For pentacene the properties of the hybrid metal-organic interface in the monolayer and the multilayer regime have been investigated for a wide range of metal substrates. It has been found that pentacene prefers to adsorb in a flat-lying geometry on metal surfaces in the monolayer regime and in either a physisorbed or weakly chemisorbed state. For pentacene on Au(111) the structure formation is dominated by long-range van der Waals interactions[6]. On Cu(111) on the other hand pentacene has shown to be chemisorbed[6,7] but compact well-ordered layers have only occasionally been reported[7].

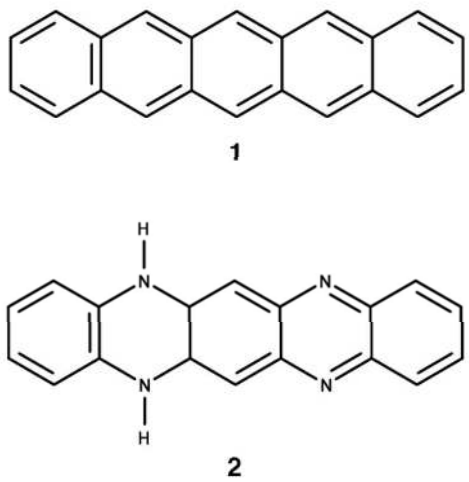

Scheme 1: Schematic representation of pentacene **1** and dihydrotetraazapentacene (DHTAP) **2**.

The situation is quite different for pentacene adsorption on the fcc(110) surfaces of coinage metals because of their anisotropic, rectangular unit cells that tend to impose a preferred orientation on elongated molecules and prevent the formation of rotational domains. For pentacene on Ag(110)[8] and Au(110)[9] the long molecular axis is oriented perpendicular to the densely packed $[\bar{1}10]$ direction. On Cu(110), however, the pentacene molecules are oriented parallel to the $[\bar{1}10]$ direction[10,11]. This important difference between adsorption on Ag(110) and Au(110) on the one hand and Cu(110) on the other can be attributed the different unit cell parameters of these three surfaces. Indeed, the nearest neighbor distance along the $[\bar{1}10]$ direction is 2.55 Å for Cu(110), which is similar to the distance between phenyl rings (2.5 Å) of pentacene, but equals 2.88 Å for Ag(110) and Au(110). The close match of the size of the phenyl rings and the Cu-Cu distances facilitates the formation of chemisorption bonds which result in a strong bending of the molecular backbone that has been observed experimentally[12] and recently confirmed by DFT calculations[13]. A variety of different substructures has been observed for pentacene on Cu(110). At 430K sample temperature during deposition the coexistence of a p(6.5x2) structure with a c(13x2) structure has been reported[14]. A p(7x2) structure and a two domain (6 1 | -1 4) structure were observed when the sample was held at room temperature during the deposition[11,15].

The quest for alternatives to pentacene was triggered by its poor long-term stability under ambient conditions[16]. In this context particular interest has recently been devoted to nitrogen-containing oligoacene derivatives such as DHTAP because of the high stability of these compounds under ambient conditions[17,18]. A previous investigation showed that the presence of the H-donor (N−H) and H-acceptor (N=C) sites in DHTAP can lead to molecule-molecule interactions via H-bonding thus promoting the formation of highly ordered molecular films on Au(111)[19]. In this case the DHTAP is physisorbed and the structure of the adsorbed layers is entirely determined by molecule-molecule interactions. We expect the behavior of DHTAP layers on Cu(110) to be very different from that on Au(111) because of presence of the imine groups, which should lead to a strong chemisorption through Cu-N bonds. This would in turn lead to a bonding mechanism which is also very different from that

of pentacene on Cu(110). Here we present a combined experimental and theoretical approach based on scanning tunneling microscopy (STM), low energy electron diffraction (LEED), and density functional theory (DFT) calculations in order to elucidate adsorption geometries, the nature of the molecule surface bond, and the superstructures for DHTAP on Cu(110).

Experimental and theoretical methods:

The experiments were carried out in an ultra-high vacuum (UHV) system with a base pressure in the 10^{-11} mbar range. The Cu(110) single crystal was cleaned by several cycles of Ar^+ sputtering and thermal annealing at about 750 K. DHTAP was thermo-evaporated from a quartz crucible heated to 500 K and deposited on the surface held at different temperatures in the range between 240 and 430 K. We define 1 ML (monolayer) in this article as the molecular density of the most compact structure which corresponds to the (6 0 | 1 2) structure (see below for details). The packing density for this structure is 0.904 molecules/nm^2. The STM experiments were performed under ultra-high vacuum (low 10^{-11} mbar) conditions using a commercial low-temperature STM (Omicron). The LT-STM was operated at liquid nitrogen temperature (78 K for both sample and tip) and using constant current mode for all experiments presented below. Low energy electron diffraction (LEED) measurements have been performed to determine the ordered molecular superstructures.

We have used density functional theory (DFT) to study the geometric and electronic properties of DHTAP on Cu(110). All calculations were performed in VASP version 5.41[20-23], which uses the projector augmented wave (PAW) method[24,25]. The substrate was modeled by 5 layer thick slabs with at least 19 Å of vacuum. On top of these the molecular superstructures were constructed for the (6 0 | 1 2), (7 0 | 1 2), and (6 -1 | 1 2) unit cells as found for different experimental conditions in this work. The molecular configuration and the substrate atoms were relaxed separately. For the lattice constant of the Cu bulk we used the calculated value of 3.626 Å[26]. Moreover, the bottom two layers of the slab were held fixed at their relaxed positions of the clean substrate before we placed the molecule on the substrate in one of four adsorption sites (see supporting information). We used a 6x6x1 KPOINT grid to sample the Brillouin zone, a 400 eV plane wave energy cut-off, and a 0.02 eV/Å force cut-off. Structural relaxation was achieved using the conjugate gradient method[27,28]. For the exchange-correlation function we chose the van der Waals inclusive optB88-vdW[29] functional. This choice was motivated by previous studies favoring this particular van der Waals inclusive functional[26,30–32]. After structural relaxation, we recorded the adsorption energy (the energy of the isolated substrate and molecules minus the energy of the molecule-substrate system), the adsorption height (the average z-coordinate of the atoms within the molecule minus the average z-coordinate of the atoms in the first layer of the substrate), the buckling of the first layer of the substrate (the maximum minus the minimum of the z-coordinates of the atoms in the first layer of the substrate), and the buckling of the molecule (the maximum minus the minimum of the z-coordinates of all atoms of the molecule). We also recorded the charge transfer to the substrate from the molecule (calculated using Bader's charge analysis[33-35]).

Results and discussion:

Figure 1a shows an STM image (at 78 K) of samples covered with 0.1 ML of DHTAP deposited on the Cu(110) surface at room temperature. Individual molecular adsorbates can be resolved and it appears that these molecules are exclusively aligned with their long molecular axis parallel to the $[\bar{1}10]$ direction. It turns out that the DHTAP molecules adsorb on the surface with their molecular planes parallel to the surface plane. Indeed, the apparent height in STM is 110 pm, which is roughly the same height found for DHTAP on Au(111) where the molecules are considered to lie flat on the surface[19]. At this low coverage we observe either isolated DHTAP molecules or small aggregates, in which the molecules arrange along the [001] direction with an intermolecular spacing of 0.722 nm that corresponds to twice the lattice spacing of the Cu(110) surface in this direction. However, neighboring molecules are shifted laterally (i.e., along the $[\bar{1}10]$ direction) by exactly one Cu-lattice spacing of 0.255 nm, leading to a stacking direction that is inclined by an angle of ±19.5° with respect to the [001] direction of the substrate. The discrete lateral shift is directly observed in the high-resolution STM images in Fig. 1b where the Cu atomic lattice is imaged concurrently with the molecules. Moreover, it is obvious that the molecules are centered between the Cu rows along the [001] direction, and thus adsorbed within the trenches rather than on top of the Cu rows. These results are similar to pentacene on Cu(110) which is isostructural to DHTAP[12], but for pentacene a parallel arrangement without a shift along the $[\bar{1}10]$ axis has also been observed for low coverage[36].

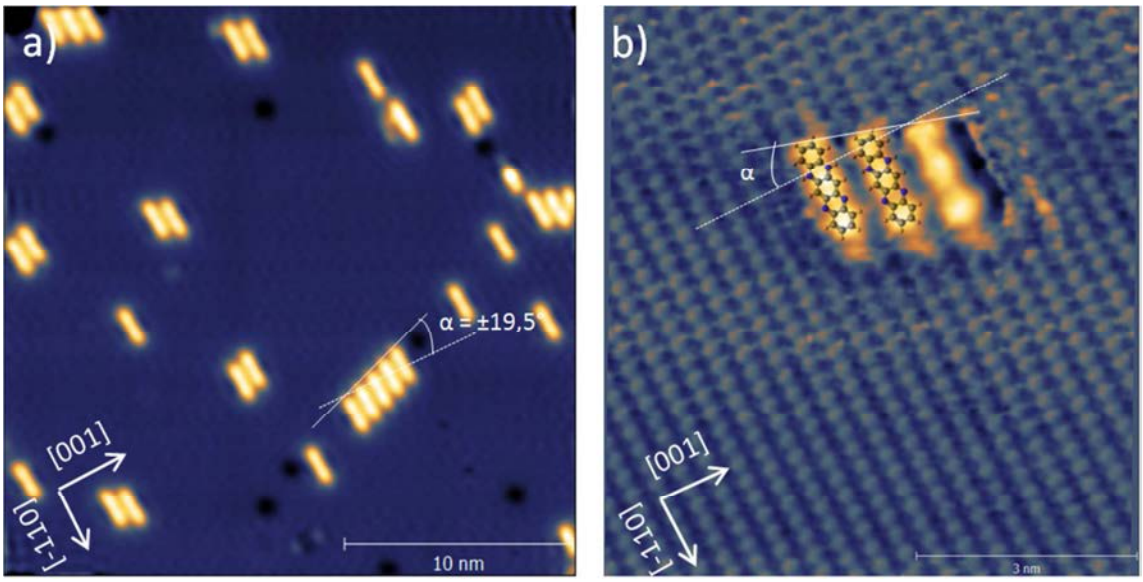

Figure 1: STM images of the Cu(110) surface covered with 0.1 ML of DHTAP adsorbed at room temperature. Individual DHTAP molecules appear as bright (yellow) rods. All molecules are aligned along the $[\bar{1}10]$ direction of the substrate. Part b) shows the atomically resolved substrate lattice with a molecular trimer, overlaid with a ball-and-stick model of the DHTAP molecules. Tunneling parameters: a) I_t = 50 pA, V_{sample} = +0.5 V and b) I_t = 6 nA, V_{sample} = -0.10 mV.

Figure 2 shows STM images of 0.35 ML and 0.5 ML of DHTAP deposited at room temperature. At the lower coverage mostly 1D stacks of molecules meandering along the [001] direction are observed with no apparent tendency for aggregation along the $[\bar{1}10]$ direction. At a coverage of 0.5 ML one starts to observe the formation of 2D islands suggesting that attractive interactions along the $[\bar{1}10]$ direction should be weak or negligible. If we zoom into these 2D islands, two distinct arrangements, as illustrated in Fig. 2c and 2d, are observed that can be assigned to commensurate superstructures with epitaxial matrices (7 0 | 1 2) and (6 -1 | 1 2), respectively. It should be noted that in both structures the molecules are stacked along the [001] direction with a shift of one Cu lattice along the $[\bar{1}10]$ direction between neighboring molecules. Consequently, mirror domains for both structures exist which can be denoted as (7 0 | -1 2) and (6 1 | -1 2), respectively. For 0.35 ML (shown in Fig. 2a), the molecular stacks are short and a considerable number of isolated molecules are found. The average length of the molecular row is 2.30 nm. The length of molecular rows increases when the coverage increases. For 0.5 ML, the average length of the molecular rows is 4.60 nm. The effect of temperature deposition was studied for molecule coverage of 0.35 ML at 240 K, 300 K and 430 K. The rows become longer with increasing deposition temperature and do not condense into larger 2D islands (see supporting information).

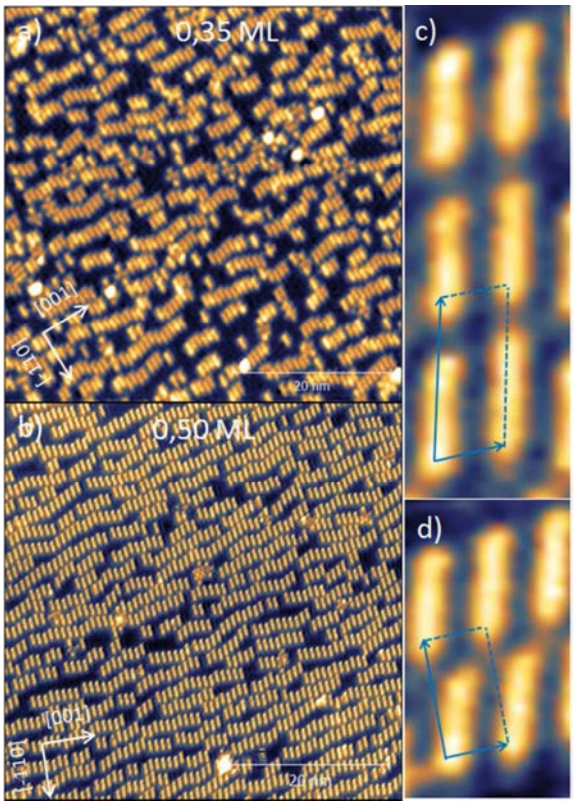

Figure 2: a) and b) STM images of the Cu(110) surface covered by 0.35 and 0.5 ML of DHTAP, respectively. The images in c) and d) show high-resolution zooms of the image shown in (b) revealing two different structures, which can be described by epitaxial matrices (7 0 | 1 2) and (6 -1 | 1 2), respectively. Tunneling parameters: $I_t = 100$ pA, $V_{sample} = +0.5$ V.

Figure 3 shows STM images for a DHTAP coverage of 0.8 ML, where the molecules were deposited at different substrate temperatures. For low deposition temperature (240 K), depicted in Fig. 3a, despite the uniaxial orientation of the DHTAP molecules, no long-range order can be observed. After deposition at 300 K (Fig. 3b) - as for the smaller coverages in Fig. 2 above – we observe small 2D islands with the same two types of superstructures: the red circles in Fig. 3b indicate areas in which the (7 0 | 1 2) structure is observed and the green circles correspond to areas with a local (6 -1 | 1 2) structure.

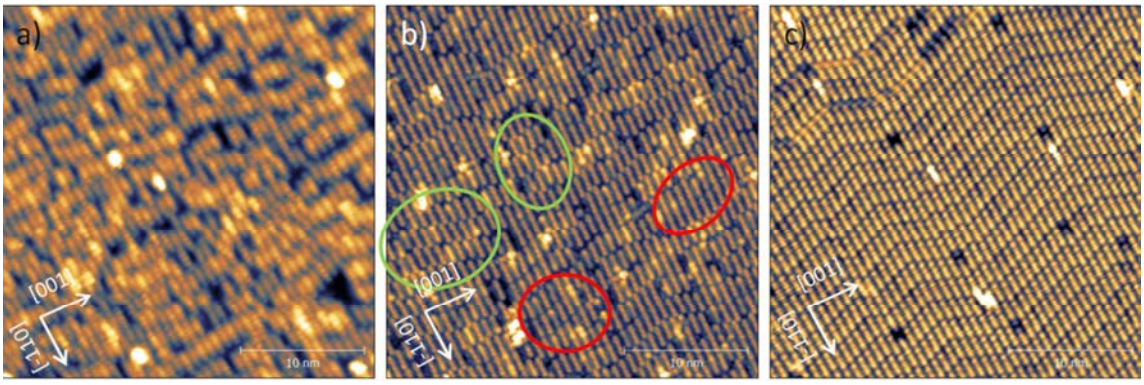

Figure 3: STM images of the Cu(110) surface covered with 0.8 ML of DHTAP deposited at a substrate temperature of 240 K (a), 300 K (b) and 430 K (c). Tunneling parameters: I_t = 100 pA, V_{sample} = +0.5 V.

Finally, for a deposition temperature of 430 K the STM image shown in Fig. 3c clearly shows the emergence of long-range order. At this temperature, the molecules form a highly ordered structure corresponding to a (7 0 | 1 2) superstructure. The theoretical packing density for this structure is 0.775 molecules/nm^2. This result is confirmed by the LEED pattern shown in Fig. 4. Along the [001] direction, bright spots at ½ of the substrate reciprocal lattice vector can be seen, which corresponds to the twofold commensurability of the real space lattice in this direction. We can also discriminate rows of spots, which are inclined by ±19.5° against the [$\bar{1}$10] direction. In order to attribute these spots, the software package LEEDpat was used to simulate the diffraction pattern based on the superstructure matrices determined by STM. The simulated LEED pattern is shown as a semitransparent overlay in the righthand part of Fig. 4. The coincidence of the simulated and the measured LEED pattern corroborates the (7 0 | 1 2) superstructure found in STM. The blue and red spots correspond to the two mirror domains, respectively.

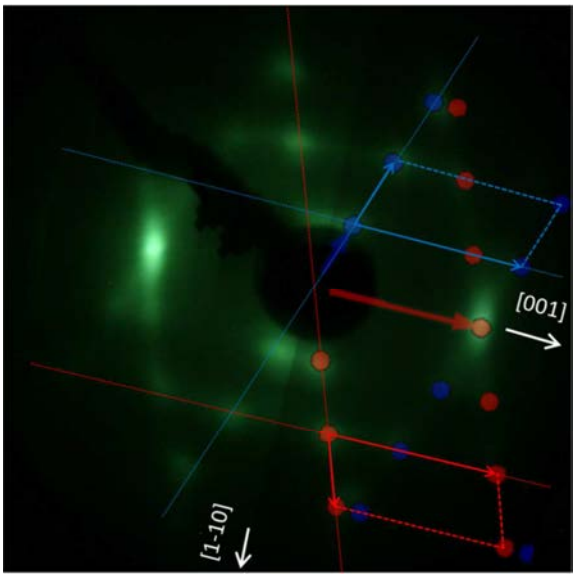

Figure 4: LEED pattern of the surface shown in Fig. 3c), acquired with an electron beam energy of 17.6 eV. In the righthand part of the image we have overlaid the spots and unit cells of simulated LEED pattern of a (7 0 | 1 2) superstructure, which fit well with the experimental data. The blue and red colors correspond to the two mirror domains, respectively.

Even though the DHTAP layer shown in Fig. 3c seems to be rather compact, it is possible to reach even higher molecular packing by further exposing the surface to DHTAP. Figure 5 shows STM images of samples covered with 1 ML of DHTAP deposited at different temperatures. Again, an inclination of ±19.5° of the short superstructure axis with respect to the [001] direction can be observed. This is markedly different from pentacene on Cu(110), which shows rows of molecules inclined by only ±9° that corresponds to a lateral shift of neighboring molecules by only half of single Cu lattice spacing along the $[\bar{1}10]$ direction. After deposition at 240K (Fig. 5a), the STM data suggest that the DHTAP molecules mostly condense into a (6 -1 | 1 2) phase with a packing density of 0.835 molecules/nm^2. Yet, at this deposition temperature, the layer shows a lot of stacking defects and there is no long-range order over scales larger than a few nm. After deposition at 430 K, in Fig. 5c, neighboring rows of molecules are mostly aligned, and the molecules appear regularly connected along the $[\bar{1}10]$ direction. The STM images can be interpreted in terms of a (6 0 | 1 2) structure with a packing density of 0.904 molecules/nm^2, which is the most compact structure that we could observe for DHTAP on Cu(110). The monolayer calibration thus refers to this molecular density. Moreover, for this structure we can see a slight undulation along the $[\bar{1}10]$ direction. The presence of both superstructures (6 -1 | 1 2) and (6 0 | 1 2), respectively, is confirmed by the LEED patterns shown in Figs. 5d and 5f, respectively. The simulated LEED patterns, corresponding to these epitaxial matrices are overlaid in the righthand part of Fig. 5d and 5f and confirm our assignments based on the STM data. The green ellipsoids in Fig. 5 indicate areas of the (6 -1 | 1 2) structure and the corresponding LEED spots whereas the red ellipsoids mark areas with a (6 0 | 1 2) structure and the corresponding LEED spots. At an intermediate deposition temperature (330 K) both superstructures are found to coexist in the same STM image (see Fig. 5b) with about 80% of the surface covered with the (6 0 | 1 2) structure.

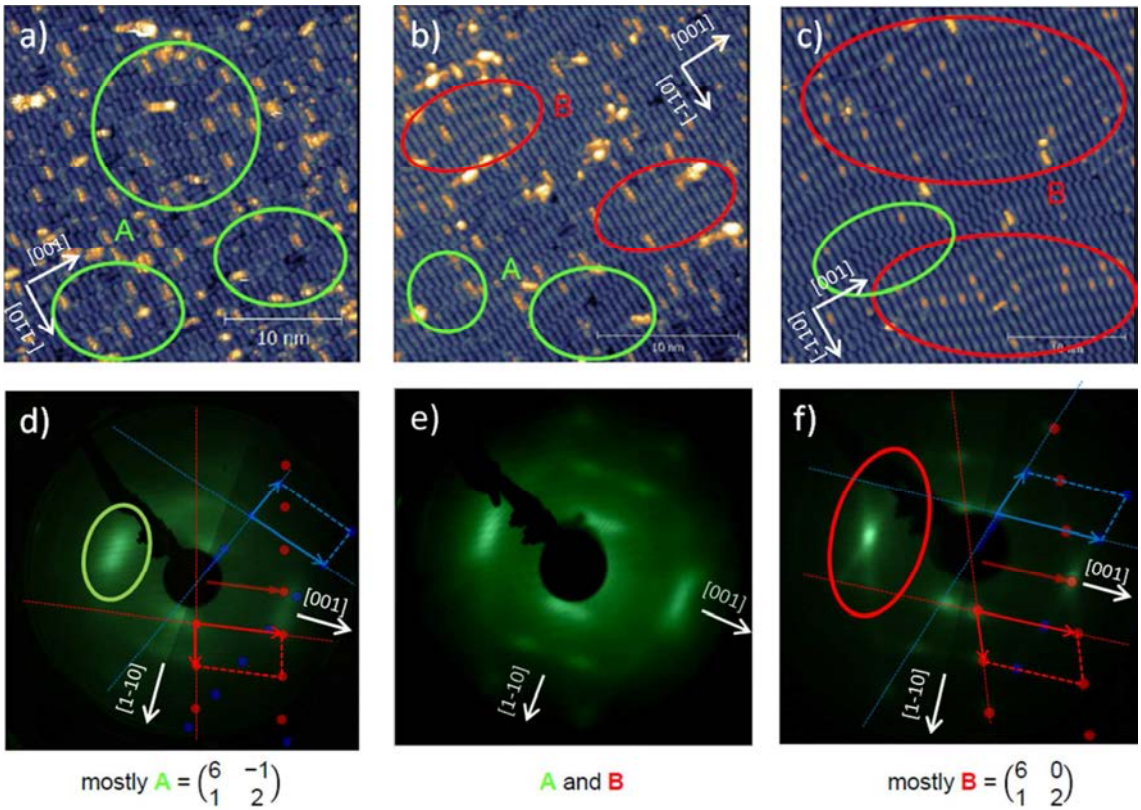

Figure 5: STM images of the Cu(110) surface covered with 1 ML of DHTAP on Cu(110) deposited at a substrate temperature of 240 K (a), 330 K (b) and 430 K (c), respectively. Tunneling parameters: I_t = 100 pA, V_{sample} = +0.5 V. d), e) and f) LEED patterns of the surfaces shown in a), b) and c), respectively, acquired with an electron beam energy of 17.6 eV. The simulated LEED patterns for the (6 -1 | 1 2) and the (6 0 | 1 2) structures are overlaid in the righthand part of d) and f), respectively. The blue and red arrows indicate the unit cell vectors for the two mirror domains. The slightly blurred spots and the rather bright background intensity indicate limited domain sizes and the presence of some disorder, respectively.

DFT calculations were performed for the three superstructures of DHTAP on Cu(110) that we observed in the STM and LEED experiments in order to determine the precise adsorption geometry of the DHTAP molecules on Cu(110). Furthermore, the calculations permit to determine the nature of the bonding between the molecules and the substrate. As expected from the STM results, the most stable configurations found with DFT correspond to DHTAP molecules that are adsorbed between the Cu rows and aligned along the $[\bar{1}10]$ direction for all three superstructures (see Fig. 6). The configuration where the DHTAP was placed on top of the densely packed Cu rows also yielded stable adsorption geometries, which were, however, systematically less stable than those in the trenches. This result is clearly confirmed by the STM image shown in Fig. 1b where the atomic resolution of the Cu lattice can be seen. Moreover, different initial positions of the DHTAP along the trenches were investigated by DFT (see supporting information). All these configurations evolved during

relaxation to sites in which the N atoms of the molecules are located close to a single Cu atom. This optimum configuration is also shown in the STM image in Fig. 1b where a ball-and-stick model of two DHTAP molecules on Cu(110) are overlaid on the STM image. We also note that in the calculations all molecules in adjacent rows are oriented with their long molecular axis parallel to the $[\bar{1}10]$ direction and not in a head-to-tail fashion as for DHTAP on Au(111)[19]. This is corroborated by the STM images in Fig. 7 where the asymmetry of the molecules is clearly visible and an identical orientation of all molecules can be seen. The particular orientation found for DHTAP on Au(111) was attributed to the presence of hydrogen bonding between adjacent rows[19], which does not seem to play a role for the DHTAP molecules on the Cu(110) surface. Here the preferred position of the N atoms of the DHTAP molecules with respect to the Cu atoms along the $[\bar{1}10]$ direction and, hence, the N-Cu interactions, seem to be the driving force for the observed adsorption geometry.

For all three superstructures shown in Fig. 6 we find relatively short N-Cu distances of roughly 2 Å (see Tab. 1). This is considerably shorter than the C-Cu distance found for pentacene on Cu(110) of 2.29 Å which has been attributed to a chemisorbed state[13]. Moreover, comparing our value with the N-Cu bond length on the Cu(100)-(2x2)N reconstructed surface, which was determined by photoelectron diffraction to be 1.99 Å[37], we can conclude that DHTAP is chemisorbed on the Cu(110) surface via the N atoms. This is corroborated by the fact that the calculated adsorption energies for DHTAP on Cu(110) are in the range of 2.93 to 3.08 eV (see Tab. 1). This is considerably higher than for the (6.5 x 2) structure of pentacene on Cu(110), which was calculated to be 1.59 eV for an isolated molecule[11]. We also note that the adsorption energy for the monolayer of pentacene, determined experimentally by thermal desorption, is 2.1 eV[14]. Moreover, an important charge transfer from the DHTAP molecule to the Cu(110) surface of -0.6e to -0.8e was found in the DFT calculations for the (6 -1 | 1 2) and the (7 0 | 1 2) structure, respectively.

The DFT calculations also suggest an important buckling of the adsorbed DHTAP molecules. A similar observation has been reported for pentacene molecules on Cu(110)[12,13], Cu(111)[38] and Al(001)[39]. In these cases, the molecules appear as dumbbell-shaped protrusions, which were assigned to a bending of the adsorbed molecule where the center of the molecule is closest to the substrate metal. The DFT calculation for the (7 0 | 1 2) structure of DHTAP on Cu(110) (see Fig. 6e) also show a bending of the molecule, which, however, is asymmetric since the N-Cu bond is not located at the center of the molecule. This result is consistent with the contrast in the STM images shown in Fig. 7b, where we have overlaid the calculated configuration of the DHTAP molecule on Cu(110) for the (7 0 | 1 2) structure. Indeed, the lowest apparent height exactly coincides with the position of the N atoms. A similar result was found for the other two structures. No asymmetry in the molecule can be seen for the (6 -1 | 1 2) structure shown in figure 7(a) but the extremities of the molecule appear brighter than the center as predicted by the DFT calculation (see Fig. 6d)). In contrast, the DFT calculations of the (6 0 | 1 2) structure reveal an s-shaped molecule (Fig. 6f)), where one end of the molecule is pointing away from the surface and the other end is rather pointing towards the surface. This is corroborated by the STM image show in Fig. 7c, which shows bright protrusions at the border between two molecules. We attribute this to the steric hindrance between the molecules, which has to be avoided in order to achieve the densest

packing along the $[\bar{1}10]$ direction. This also induces a slight rotation of the molecules out of the $[\bar{1}10]$ direction, which is found in the DFT calculations and can also be recognized in the STM images in Figs. 5c and 7c.

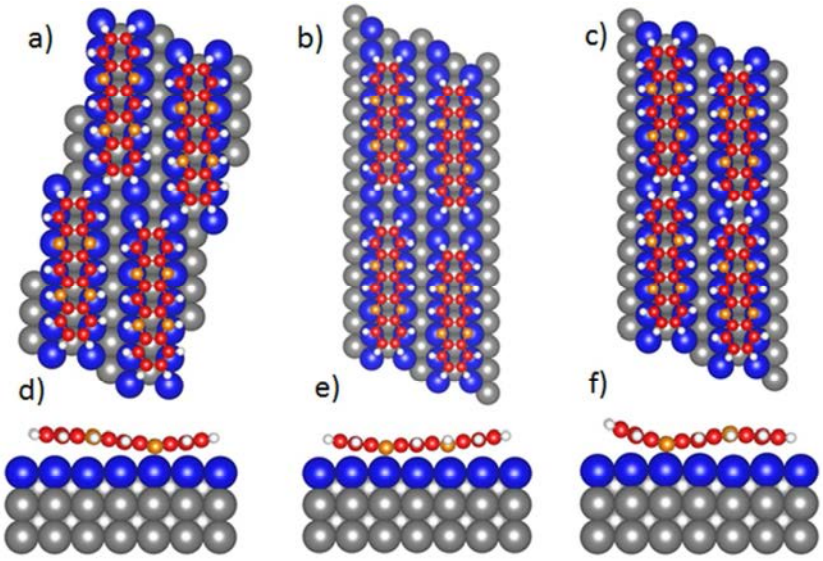

Figure 6: Calculated DHTAP adsorption configurations on Cu(110) for the (6 -1 | 1 2), (7 0 | 1 2) and (6 0 | 1 2) structure. Red: C atoms, orange: N atoms, white: H atoms, blue: Cu atoms of the first layer and gray: Cu atoms of the bulk. a), b) and c): top views of the (6 -1 | 1 2), (7 0 | 1 2) and (6 0 | 1 2) structures, respectively. The N atoms of the molecules are located on top of the Cu atoms of the first layer; d), e) and f): side views illustrating the bending of the molecules.

Table 1: Adsorption parameters determined from the DFT calculations for each of the three superstructures of DHTAP on Cu(110): adsorption energies, adsorption height, shortest N-Cu distance, buckling of the first layer of the substrate and of the molecule, charge transfer to the substrate.

Structure	Adsorption energy (eV)	Surface adsorption energy (eV/nm^2)	Adsorption height (Å)	N-Cu distance (Å)	Buckling of the first layer of the substrate (Å)	Buckling of the molecule (Å)	Charge transfer (e)
(7 0 | 1 2)	3.08	2.39	2.46	2.04	0.1	0.92	-0.8
(6 -1 | 1 2)	2.93	2.45	2.58	2.05	0.15	0.98	-0.6
(6 0 | 1 2)	3.04	2.75	2.59	2.02	0.2	1.5	-0.7

The buckling of the first layer of the substrate and the buckling of the molecules are smallest for the (7 0 | 1 2) structure, which, however, is the structure with the highest adsorption energy per molecule. The lower buckling can be explained by the fact that the (7 0 | 1 2) structure is the least compact adsorption configuration especially in the $[\bar{1}10]$ direction, yielding only weak steric hindrance between neighboring molecules. If we turn our attention to the surface adsorption energies, which are calculated from the adsorption energies per molecule and the area of the corresponding superstructure unit cell, we can see that the (7 0 | 1

2) and the (6 -1 | 1 2) structure are energetically almost equivalent with values of 2.39 eV/nm^2 and 2.45 eV/nm^2, respectively. This rather nicely explains the coexistence of these two structures at a deposition temperature of 300 K and a coverage of 0.8 ML of DHTAP. We can also conclude that the (6 0 | 1 2), which is found in the monolayer is by far the structure with the lowest surface energy. The fact that this most densely packed structure is not observed for low deposition temperatures points to the existence of an activation barrier for the formation of this structure. This could be due to the important steric hindrance between molecules, which has to be overcome upon compression along in the $[\bar{1}10]$ direction.

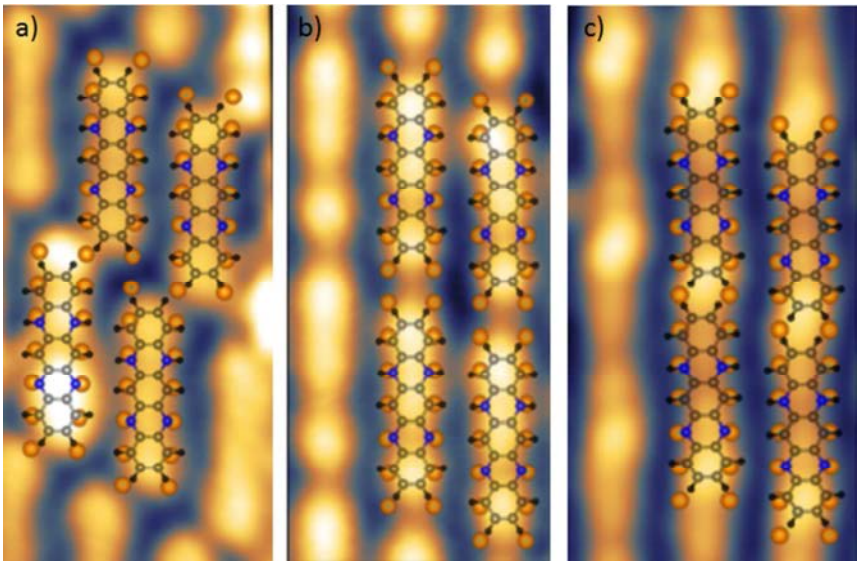

Figure 7: High-resolution STM images of the a) (6 -1 | 1 2), b) (7 0 | 1 2) and c) (6 0 | 1 2) structure of DHTAP on Cu(110). Tunneling parameters: I_t = 100 pA, V_{sample} = +0.5 V, scale: (2.2 x 4.2) nm^2. Overlaid are the adsorption configurations obtained from the DFT calculation for each of the three structures.

Conclusion

We have investigated the adsorption of DHTAP on Cu(110) in the monolayer regime and for different deposition temperatures. The molecules adopt a flat-lying adsorption geometry with their long molecular axes oriented parallel to the $[\bar{1}10]$ direction. The DHTAP molecules are centered in the trenches between the close-packed Cu rows with the N atoms of the molecule located on top of the Cu atoms of the first layer. The Cu-N bond length is comparable to that found for the Cu(100)-(2x2)N surface indicating strong chemisorption. Unlike for pentacene, for which the bonding is delocalized, the dominant contribution to bonding comes from the Cu-N bond. We could identify three different commensurate adsorption structures of DHTAP on Cu(110), which can be described by the epitaxial matrices (7 0 | 1 2), (6 -1 | 1 2), and (6 0 | 1 2), respectively.

Supporting information

Initial geometries for DFT calculations. STM images of 0.35ML DHTAP layers at various temperatures.

Acknowledgment

The authors gratefully acknowledge the financial support from the Agence Nationale de la Recherche through grant ANR 14 CE34 0003 01 and Campus France through grant PHC AMADEUS 2017 38069TB. P.Z. gratefully acknowledges the support from AMU Marseille through an invited professorship and the CNRS via a research fellowship with the CINaM during a sabbatical leave in 2016. The work of A.K. and W.M. is supported by a grant from the U.S. Department of Energy Basic Energy Science under Contract No DE-FG02-11ER16243. A.K. and W.M. also acknowledge the University of Central Florida Stokes Advanced Research Computing Center for providing computational resources and support that have contributed to the computational results reported herein.

References

(1) Witte, G.; Wöll, C. Growth of Aromatic Molecules on Solid Substrates for Applications in Organic Electronics. *J. Mater. Res.* **2004**, *19*, 1889–1916.

(2) Horowitz, G. Organic Thin Film Transistors: From Theory to Real Devices. *J. Mater. Res.* **2004**, *19*, 1946–1962.

(3) Di, C. A.; Zhang, F.; Zhu, D. Multi-Functional Integration of Organic Field-Effect Transistors (OFETs): Advances and Perspectives. *Adv. Mater.* **2013**, *25*, 313–330.

(4) Kelley, T. W.; Baude, P. F.; Gerlach, C.; Ender, D. E.; Muyres, D.; Haase, M. A.; Vogel, D. E.; Theiss, S. D.; Recent Progress in Organic Electronics: Materials, Devices, and Processes. Chem. Mater. **2004**, *16*, 4413-4423.

(5) Koch, N. Organic Electronic Devices and Their Functional Interfaces. *Chem. Phys. Chem*. **2007**, *8*, 1438-1455.

(6) Toyoda, K.; Hamada, I.; Lee, K.; Yanagisawa, S.; Morikawa, Y. Density Functional Theoretical Study of Pentacene/Noble Metal Interfaces with van der Waals Corrections: Vacuum Level Shifts and Electronic Structures. *J. Chem. Phys.* **2010***, 132*, 134703.

(7) Smerdon, J. A.; Bode, M.; Guisinger, N. P.; Guest, J. R. Monolayer and bilayer pentacene on Cu(111). *Phys. Rev. B* **2011**, *84*, 165436.

(8) Wang, Y. L.; Ji, W.; Shi, D. X.; Du, S. X.; Seidel, C.; Ma, Y. G.; Gao, H.-J.; Chi, L. F.; Fuchs, H. Structural Evolution of Pentacene on a Ag(110) Surface. *Phys. Rev. B* **2004**, *69*, 75408.

(9) Bavdek, G.; Cossaro, A.; Cvetko, D.; Africh, C.; Blasetti, C.; Esch, F.; Morgante, A.; Floreano, L.; Tasc, C. L. N.; Ss-, B.; *et al.* Pentacene Nanorails on Au(110). *Langmuir* **2008**, *24*, 767–772.

(10) Chen, Q.; Mcdowall, a J.; Richardson, N. V. Ordered Structures of Tetracene and Pentacene on Cu(110) Surfaces. *Langmuir* **2003**, *19*, 10164–10171.

(11) Zhang, L.; Liu, C. Y.; Fu, X.; Sun, L. D.; Zeppenfeld, P. Pentacene/Cu(110) Interface Formation Monitored by in Situ Optical Spectroscopy. *Phys. Rev. B* **2014**, *89*, 035428.

(12) Müller, K.; Kara, A.; Kim, T. K.; Bertschinger, R.; Scheybal, A.; Osterwalder, J.; Jung, T. A. Multimorphism in Molecular Monolayers: Pentacene on Cu(110). *Phys. Rev. B* **2009**, *79*, 245421.

(13) Müller, K.; Seitsonen, A. P.; Brugger, T.; Westover, J.; Greber, T.; Jung, T.; Kara, A. Electronic Structure of an Organic/Metal Interface: Pentacene/Cu(110). *J. Phys. Chem.* **2012**, *116*, 23465–23471

(14) Söhnchen, S.; Lukas, S.; Witte, G. Epitaxial Growth of Pentacene Films on Cu(110). *J. Chem. Phys.* **2004**, *121*, 525–534.

(15) Martínez-Blanco, J.; Ruiz-Osés, M.; Joco, V.; Sayago, D. I.; Segovia, P.; Michel, E. G. Ordered Structures of Pentacene on Cu(110). *J. Vac. Sci. Technol. B* **2009**, *27*, 863-867.

(16) Maliakal, A.; Raghavachari, K.; Katz, H.; Chandross, E.; Siegrist, T. Photochemical Stability of Pentacene and a Substituted Pentacene in Solution and in Thin Films. *Chem. Mater.* **2004**, *16*, 4980–4986.

(17) Gao, B.; Wang, M.; Cheng, Y.; Wang, L.; Jing, X.; Wang, F. Pyrazine-Containing Acene-Type Molecular Ribbons with up to 16 Rectilinearly Arranged Fused Aromatic Rings. *J. Am. Chem. Soc.* **2008**, *130*, 8297–8306.

(18) Bunz, U. H. F.; Engelhart, J. U.; Lindner, B. D.; Schaffroth, M. Large N-Heteroacenes: New Tricks for Very Old Dogs? *Angew. Chemie - Int. Ed.* **2013**, *52*, 3810–3821.

(19) Lelaidier, T.; Leoni, T.; Arumugam, P.; Ranguis, A.; Becker, C.; Siri, O. Highly Ordered Molecular Films on Au(111): The N-Heteroacene Approach. *Langmuir* **2014**, *30*, 5700–5704.

(20) Kresse, G.; Furthmüller, J. Efficient Iterative Schemes for Ab Initio Total-Energy Calculations Using a Plane-Wave Basis Set. *Phys. Rev. B* **1996**, *54*, 11169–11186.

(21) Kresse, G.; Furthmüller, J. Efficiency of Ab-Initio Total Energy Calculations for Metals and Semiconductors Using a Plane-Wave Basis Set. *Comput. Mater. Sci.* **1996**, *6*, 15–50.

(22) Kresse, G.; Hafner, J. Ab Initio Molecular Dynamics for Liquid Metals. *Phys. Rev. B* **1993**, *47*, 558–561.

(23) Blöchl, P. E. Projector Augmented-Wave Method. *Phys. Rev. B* **1994**, *50*, 17953–17979.

(24) Joubert, D. From Ultrasoft Pseudopotentials to the Projector Augmented-Wave Method. *Phys. Rev. B* **1999**, *59*, 1758–1775.

(25) Yildirim, H.; Greber, T.; Kara, A. Trends in Adsorption Characteristics of Benzene on Transition Metal Surfaces: Role of Surface Chemistry and van Der Waals Interactions.

J. Phys. Chem. C **2013**, *117*, 20572–20583.

(26) Hestenes, M. R.; Stiefel, E. Methods of Conjugate Gradients for Solving Linear Systems. *J. Res. Natl. Bur. Stand.* **1952**, *49*, 409-436.

(27) Teter, M. P.; Payne, M. C.; Allan, D. C. Solution of Schrodinger's Equation for Large Systems. *Phys. Rev. B* **1989**, *40*, 12255–12263.

(28) Klimeš, J.; Bowler, D. R.; Michaelides, A. Chemical Accuracy for the van der Waals Density Functional. *J. Phys.: Condens. Matter* **2010**, *22,* 022201.

(29) Yildirim, H.; Kara, A. Effect of van Der Waals Interactions on the Adsorption of Olympicene Radical on Cu(111): Characteristics of Weak Physisorption versus Strong Chemisorption. *J. Phys. Chem. C* **2013**, *117*, 2893–2902.

(30) Yildirim, H.; Matos, J.; Kara, A. Role of Long-Range Interactions for the Structure and Energetics of Olympicene Radical Adsorbed on Au(111) and Pt(111) Surfaces. *J. Phys. Chem. C* **2015**, *119*, 25408–25419.

(31) Matos, J.; Yildirim, H.; Kara, A. Insight into the Effect of Long Range Interactions for the Adsorption of Benzene on Transition Metal (110) Surfaces. *J. Phys. Chem. C* **2015**, *119*, 1886–1897.

(32) Tang, W.; Sanville, E.; Henkelman, G. A Grid-Based Bader Analysis Algorithm without Lattice Bias. *J. Phys.: Condens. Matter* **2009**, *21,* 084204.

(33) Truhlar, D. G. Valence Bond Theory for Chemical Dynamics. *J. Comput. Chem.* **2009**, *28*, 73–86.

(34) Henkelman, G.; Arnaldsson, A.; Jónsson, H. A Fast and Robust Algorithm for Bader Decomposition of Charge Density. *Comput. Mater. Sci.* **2006**, *36*, 354–360.

(35) Lukas, S.; Witte, G.; Wöll, C. Novel Mechanism for Molecular Self-Assembly on Metal Substrates: Unidirectional Rows of Pentacene on Cu(110) Produced by a Substrate-Mediated Repulsion. *Phys. Rev. Lett.* **2002**, *88*, 283011–283014.

(36) Hoeft, J. T.; Polcik, M.; Kittel, M.; Terborg, R.; Toomes, R. L.; Kang, J.-H.; Woodruff, D. P. Photoelectron Diffraction Structure Determination of Cu(100)c(2×2)-N. *Surf. Sci.* **2001**, *492*, 1–10.

(37) Lagoute, J.; Kanisawa, K.; Fölsch, S. Manipulation and Adsorption-Site Mapping of Single Pentacene Molecules on Cu(111). *Phys. Rev. B* **2004**, *70*, 245415.

(38) Baby, A.; Fratesi, G.; Vaidya, S. R.; Patera, L. L.; Africh, C.; Floreano, L.; Brivio, G. P. Anchoring and Bending of Pentacene on Aluminum (001). *J. Phys. Chem. C* **2015**, *119*, 3624–3633.